UC Irvine
UC Irvine Previously Published Works

Title
Frequency-domain multichannel optical detector for noninvasive tissue spectroscopy and oximetry

Permalink
https://escholarship.org/uc/item/5016j8w7

Journal
Optical Engineering, 34(1)

ISSN
0091-3286

Authors
Fantini, Sergio
Franceschini, Maria-Angela
Maier, John S
et al.

Publication Date
1995

DOI
10.1117/12.183988

Copyright Information
This work is made available under the terms of a Creative Commons Attribution License, availalbe at https://creativecommons.org/licenses/by/4.0/

Peer reviewed

eScholarship.org Powered by the California Digital Library
University of California

Frequency-domain multichannel optical detector for noninvasive tissue spectroscopy and oximetry

Sergio Fantini,* MEMBER SPIE
Maria Angela Franceschini-Fantini,* MEMBER SPIE
John S. Maier
Scott A. Walker
University of Illinois at Urbana-Champaign
Department of Physics
Laboratory for Fluorescence Dynamics
1110 West Green Street
Urbana, Illinois 61801-3080
E-mail: lfdwmeg@ux1.cso.uiuc.edu

Beniamino Barbieri, MEMBER SPIE
ISS, Incorporated
2604 North Mattis Avenue
Champaign, Illinois 61821

Enrico Gratton
University of Illinois at Urbana-Champaign
Department of Physics
Laboratory for Fluorescence Dynamics
1110 West Green Street
Urbana, Illinois 61801-3080

Abstract. We have designed a multisource frequency-domain spectrometer for the optical study of biological tissues. Eight multiplexed, intensity-modulated LEDs are employed as the light sources. Four of them emit light at a peak wavelength of 715 nm (λ_1); the other four, 850 nm (λ_2). The frequency of intensity modulation is 120 MHz. This instrument measures the frequency-domain parameters phase, dc intensity, and ac amplitude at the two wavelengths λ_1 and λ_2 and for different distances between light source and detector. From these frequency-domain raw data, the absolute values of the absorption and reduced scattering coefficients of tissue at λ_1 and λ_2 are obtained. The oxy- and deoxyhemoglobin concentrations, and hence the hemoglobin saturation, are then analytically derived from the molar extinction coefficients. Acquisition times as short as hundreds of milliseconds provide real-time monitoring of the measured parameters. We performed a systematic test *in vitro* to quantify the precision and accuracy of the instrument reading. We also report *in vivo* measurements. This spectrometer can be packaged as a compact portable unit.

Subject terms: photon migration; diffusion theory; frequency-domain spectroscopy; multiplexing circuit; biological tissue; absorption and scattering coefficients; oxygenated and deoxygenated hemoglobin; hemoglobin saturation.

Optical Engineering 34(1), 32–42 (January 1995).

1 Introduction

The determination of the optical properties of tissues is of fundamental importance in many fields in medicine for both diagnostics and monitoring.[1] Different wavelengths of light penetrate tissue preferentially. In the near infrared region, ranging from 700 to 900 nm, light penetrates several centimeters. Consequently, spectroscopic methods can, in principle, be used to measure the concentration of typical tissue constituents, such as hemoglobin, which present absorption bands in that spectral region. The most important characteristic of every apparatus aimed at the measurement of optical properties of tissues is that is must provide quantitative information about a medically important parameter, for example, the concentration of oxygenated and deoxygenated hemoglobin, of glucose, or of other typical tissue constituents.

In standard spectroscopic practice, when light extinction is mainly due to absorption, the absolute determination of the concentration of an absorber can be obtained by a measurement of the light transmitted through a sample of known thickness. A transmission measurement enables one to determine the absorption coefficient from the Beer-Lambert law. The concentration of the absorber can be calculated using the molar extinction coefficient of the absorber. If more than one absorber is present, measurements at different wavelengths can provide a method to determine the concentration of all different noninteracting absorbing chemical species present in solution, provided they have different absorption spectra. The success of this method depends on the precision of the measurement and on the number of different substances that are present.

In tissue spectroscopy the problem is more complex. A measurement of the light transmitted through a slab of tissue is not possible using noninvasive methods, except for special thin regions of the body. Moreover, the amount of transmitted light depends not only on the absorption of the medium, but also on its scattering properties. This fact is particularly important when, as for most tissues in the near infrared, the scattering coefficient far exceeds the absorption coefficient. Several different methods have been proposed to take account of the scattered light. For example, empirical corrections based on the type of tissue have been used to take into account the effect of scattering on the absorption properties.[2] Reflectance spectrophotometry has been performed,[3] and theoretical models have been used to calculate the diffuse reflectance of light from tissues.[4] The success of these methods has been marginal, although there are a number of commercial instruments based on them. The major problem with the proposed approaches is that, in order to obtain a reasonable estimate of the concentration of a substance in tissue, some sort of *a priori* calibration must be performed, based on the statistical analysis of a large number of samples. In practice, unpredictable results are frequently obtained. Instead, an ideal instrument should provide absolute and accurate values

*Also with Istituto di Elettronica Quantistica–Consiglio Nazionale delle Ricerche, Via Panciatichi, 56/30, 50127 Firenze, Italy.

Paper 12044 received April 8, 1994; revised manuscript received July 12, 1994; accepted for publication July 14, 1994.
© 1995 Society of Photo-Optical Instrumentation Engineers. 0091-3286/95/$6.00.

Downloaded From: http://proceedings.spiedigitallibrary.org/ on 08/29/2016 Terms of Use: http://spiedigitallibrary.org/ss/termsofuse.aspx

of the concentration of chromophores, independently of factors such as the color of the skin or the amount of lipids in the tissue.

A few years ago, a new approach was proposed to determine the optical properties of tissues.[5–8] The basic idea is to use time-resolved methods to separate scattering from absorption. The time-resolved measurements can be made in either the time domain or the frequency domain. In the time domain one measures the time-of-flight distribution of a light pulse between a source optical fiber and a detector fiber.[9] In the frequency domain one measures the phase delay of asinusoidally modulated light source between the source and the detector, and the attenuation of the average intensity and of the amplitude of the intensity oscillations.[10] It has been shown that, under some assumptions, the average time of flight is equivalent to a phase delay measurement at a given frequency.[11] The major advance came from the development of a rigorous mathematical model for the description of light transport in turbid media, which allowed for a better understanding of how the measurable parameters in time-resolved spectroscopy are related to the scattering and absorption coefficients of the medium.[5,12] This model is based on the assumption that the distribution of photons in strongly scattering media is well described using diffusion theory.

In the near infrared, low-cost sources such as light-emitting diodes can be modulated at frequencies high enough to realiably measure the optical parameters of tissues.[13] Using the frequency-domain method and the diffusion theory, the absorption spectrum of a chromophore was quantitatively recovered even in the presence of a concentration of scattering particles similar to those found in tissues.[14] Furthermore, we have shown that the accuracy of a measurement is increased if several source-detector separations are employed.[14] The case of a semi-infinite geometry, which is a model of the noninvasive *in vivo* configuration, has been studied both in the time domain[5] and in the frequency domain.[15] As a result, the relationships between the phase and attenuation of the photon density wave on one hand and the optical properties of the medium on the other have been determined for such a boundary condition.

In the present paper, we describe an LED-based frequency-domain spectrometer for the direct determination of the oxy- and deoxyhemoglobin content in tissues. Once the concentrations of these two chemical species are separately known, the amount of hemoglobin saturation and tissue hemoglobin content can be determined. The principle presented here is not limited to the measurement of these two substances, but can be extended to the measurement of other chromophores by properly choosing the wavelengths of the light sources. We also conducted an experimental test to study precision and accuracy of the instrument.

2 Description of the Instrument

We designed a frequency-domain spectrometer for direct measurement of oxy- and deoxyhemoglobin content in tissue based on the following features:

1. *Measurement at two wavelengths:* The determination of the concentration of two chemical species, namely oxy- and deoxyhemoglobin, requires the measurement of the absorption coefficient at a minimum of two different wavelengths.
2. *LEDs as the intensity-modulated light sources:* LEDs are attractive light sources for practical applications because of their safety, reliability, ease of modulation, stable output, and low cost.[13]
3. *Multiple source-detector separations:* A simple method to measure the absolute values of the scattering and absorption coefficients is to determine the slopes of the straight lines associated with dc, ac, and phase. The linear relationships between measurable quantities in frequency-domain spectroscopy and the source-detector distance r have been derived elsewhere.[15] For convenience, we report a brief summary of the derivation in the appendix. The measurement of the slopes of these straight lines as a function of r requires several (at least two) source-detector separations;
4. *Appropriate modulation frequency:* A frequency-domain spectrometer requires the intensity of the light source to be modulated at a certain radio frequency. The value of that frequency affects the sensitivity of the instrumentation and the signal-to-noise ratio, and hence must be chosen with care.

We designed the instrument by careful consideration of each one of the four above features.

Feature 1 Our specific goal is to determine the concentrations of the oxygenated ($[HbO_2]$) and deoxygenated ($[Hb]$) forms of hemoglobin using the methods we previously developed for the measurement of the optical parameters μ_a (absorption coefficient) and μ_s' (reduced scattering coefficient) in tissues. We assume that the main contribution to absorption in tissues in the near infrared region is due to hemoglobin, thus writing

$$\mu_a^\lambda = \varepsilon_{HbO_2}^\lambda [HbO_2] + \varepsilon_{Hb}^\lambda [Hb] \ , \tag{1}$$

where $\varepsilon_{HbO2}^\lambda$ and ε_{Hb}^λ are the extinction coefficients at wavelength λ for oxy- and deoxyhemoglobin respectively. For example, this assumption is valid for wavelengths in the near infrared for the mammalian brain, where the contribution of myoglobin and of other tissue constituents is minimal.[16,17] Equation (1) clearly shows that a single measurement is not sufficient to provide both $[HbO_2]$ and $[Hb]$. Instead, both species can be determined by measuring the absorption coefficient at two different wavelengths λ_1 and λ_2. The two equations for $\mu_a^{\lambda 1}$ and $\mu_a^{\lambda 2}$ then yield the following equations:

$$[HbO_2] = \frac{\mu_a^{\lambda 1}\varepsilon_{Hb}^{\lambda 2} - \mu_a^{\lambda 2}\varepsilon_{Hb}^{\lambda 1}}{\varepsilon_{HbO_2}^{\lambda 1}\varepsilon_{Hb}^{\lambda 2} - \varepsilon_{HbO_2}^{\lambda 2}\varepsilon_{Hb}^{\lambda 1}} \ , \tag{2}$$

$$[Hb] = \frac{\mu_a^{\lambda 2}\varepsilon_{HbO_2}^{\lambda 1} - \mu_a^{\lambda 1}\varepsilon_{HbO_2}^{\lambda 2}}{\varepsilon_{HbO_2}^{\lambda 1}\varepsilon_{Hb}^{\lambda 2} - \varepsilon_{HbO_2}^{\lambda 2}\varepsilon_{Hb}^{\lambda 1}} \ . \tag{3}$$

We want to perform measurements in the spectral region from 700 to 900 nm, in which light transmission is sufficient to provide both a large penetration depth (several centimeters) and an acceptable detected intensity. At shorter wavelengths ($\lambda < 700$ nm) the extinction coefficient of hemoglobin becomes much higher,[18] thus limiting penetration. At longer wavelengths ($\lambda > 900$ nm) the absorption of water domi-

Downloaded From: http://proceedings.spiedigitallibrary.org/ on 08/29/2016 Terms of Use: http://spiedigitallibrary.org/ss/termsofuse.aspx

nates.[19] We also want to minimize the errors in $[HbO_2]$ and [Hb], which are related to the experimental uncertainties in the determination of $\mu_a^{\lambda_1}$ and $\mu_a^{\lambda_2}$ as stated by Eqs. (2) and (3). From Eqs. (2), (3) and from the extinction-coefficient spectra of oxy- and deoxyhemoglobin,[18] it follows that the smallest errors in $[HbO_2]$ and [Hb] occur for $\lambda_1 = 700$ nm and $\lambda_2 = 850$ to 900 nm. This result is shown in Fig. 1, where the errors in $\mu_a^{\lambda_1}$ and $\mu_a^{\lambda_2}$ are set equal to 0.001 cm^{-1}.

Feature 2. The feasibility of using LEDs as light sources in frequency-domain tissue spectroscopy has already been shown.[13] Commercially available LEDs cover the optical window from 700 to 900 nm almost continuously. We chose two emission wavelengths that maximize the precision of the measurement of $[HbO_2]$ and [Hb]. The LEDs used were the following:

1. LED Hewlett Packard HEMT-6000 ($\lambda_1^{peak} = 715$ nm),
2. LED Motorola MFOE1203 ($\lambda_2^{peak} = 850$ nm).

These LEDs can be efficiently modulated up to about 120 MHz by driving them with a low-voltage oscillating signal. We emphasize that the average optical power emitted by LEDs is usually less than a few milliwatts and is distributed over a wide solid angle. These properties make LEDs particularly safe in medical applications. The emission from LEDs has different ANSI standards than the emission from lasers.

Feature 3. To implement the measurement of the slopes of the straight lines (as a function of the distance r between source and detector) associated with dc, ac, and phase, we have designed a spectrometer that employs eight different light sources placed at different distances from the detector fiber bundle, as shown in Fig. 2. The detector fiber bundle (3 mm in diameter, 0.56 numerical aperture) is connected to a photomultiplier tube. The eight sources are arranged in two parallel rows of four LEDs: in the first (second) row we placed the 715-nm (850-nm) LEDs, so that each row implements the measurement of the slopes at one wavelength. The source-detector distances in each row range from 1.5 to 3.5 cm, and a light shield is placed between sources and detector to prevent reflected light from being detected. The two rows are placed as close as possible to each other in order to explore essentially the same region of the sample. The eight sources are turned on one at a time in rapid succession, using the multiplexer circuit shown in Fig. 3. The clock signal from the computer (whose frequency can be selected by software and is synchronous with the cross-correlation frequency introduced in the following paragraph) is the input of a counter (RCA CD4024), which drives a demultiplexer (RCA 74HCT238) with eight outputs connected to eight relays (Magnecraft W171DIP-2). The relays, which are closed one at a time, are in series with each LED. The result is that the LEDs are turned on in sequence at the frequency of the clock. In order to start the sequence always with the same LED, the counter is reset by a pulse sent by the computer at the beginning of the measurement. Resistors R_1 to R_8 in Fig. 3 are added to decrease the current in some of the light sources in order to have comparable light intensities at the detector fiber from each LED. This procedure of light-source equilibration allowed us to use the entire dynamic range of the analog-to-digital converter.

Feature 4. The light sources are sinusoidally modulated at a frequency of 120 MHz. This frequency provides the best compromise among the three requirements of high modulation of the source, high sensitivity of our detector (photomultiplier tube, Hamamatsu R928), and high sensitivity of

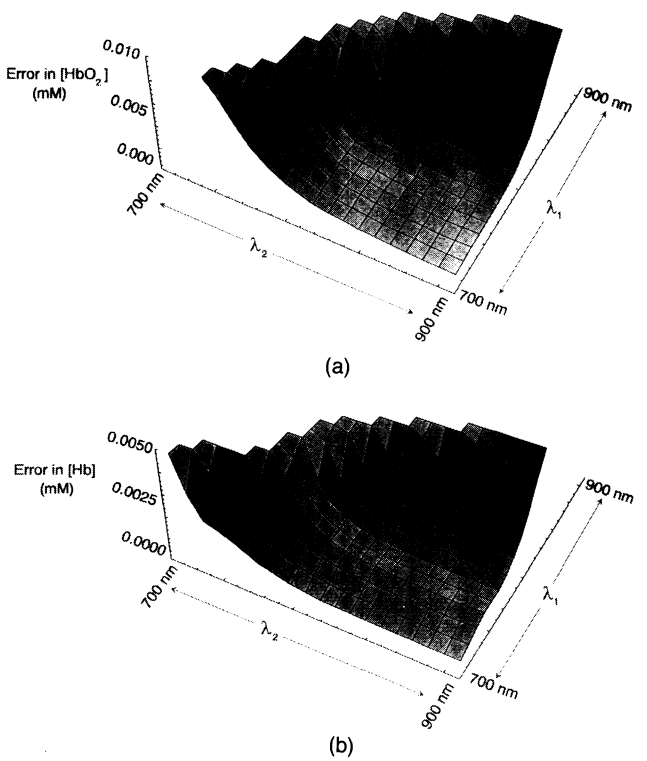

Fig. 1 Errors in (a) $[HbO_2]$ and (b) [Hb] as a function of the two wavelengths employed (λ_1,λ_2). The values of the standard errors in $\mu_a^{\lambda_1}$ and $\mu_a^{\lambda_2}$ have been set equal to 0.001 cm^{-1}.

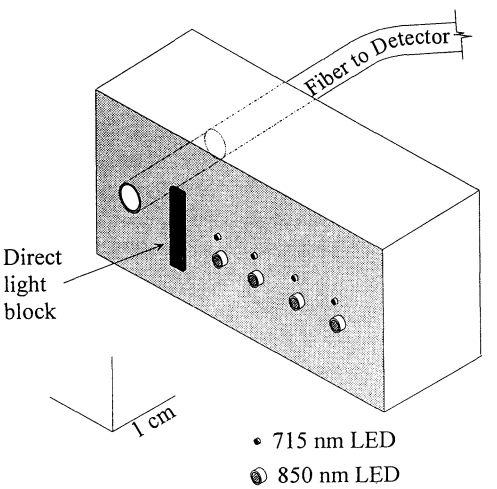

Fig. 2 Design of the measuring head of the tissue spectrometer. In a measurement, the shaded surface, on which the eight LEDs and the tip of the detector optical fiber are located, is placed in contact with the sampled medium. The light shield between sources and detector is used to block the light reflected at the surface of the medium.

Downloaded From: http://proceedings.spiedigitallibrary.org/ on 08/29/2016 Terms of Use: http://spiedigitallibrary.org/ss/termsofuse.aspx

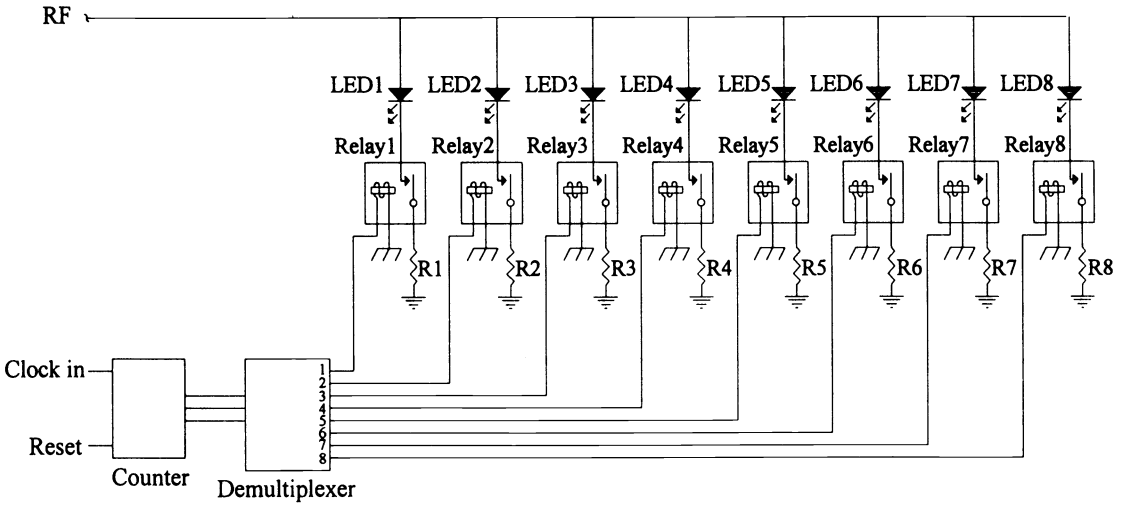

Fig. 3 Schematic diagram of the measuring head circuit. The inputs are the radio-frequency oscillating signal (from a frequency synthesizer), a clock signal, and a reset pulse (both from the computer). The counter (RCA CD4024) counts the waves of the clock signal and continuously transmits the number (mod 8) to the demultiplexer (74HCT238). The enabled line of the demultiplexer, which closes the corresponding relay (Magnecraft W171 DIP-2), is then changed at the frequency of the clock. The reset pulse is sent at the beginning of the measurement to start the sequence always with the same LED.

the measured quantities (slopes S_{dc}, S_{ac}, S_{Φ}) to the absorption and scattering coefficients. The photomultiplier-tube gain is modulated at a frequency of 120.0004 MHz. This method produces a beating of the 120-MHz modulated current in the detector photomultiplier with the 120.0004-MHz radio-frequency signal injected at the photomultiplier second dynode, as shown in the instrument block diagram of Fig. 4. The photomultiplier-tube output is fed to an ISS Model A2D data acquisition card inserted in the personal computer, featuring current-to-voltage converters, signal amplification stage, and a 12-bit analog-to-digital converter. The 400-Hz low-frequency component of the photomultiplier output—the cross-correlation frequency—is isolated by using a variable-bandwidth digital filter and is digitized through a fast Fourier transform routine.

Each of the eight light sources is turned on for a time that is an exact multiple of the 400-Hz wave period, i.e., a multiple of 2.5 ms. In a typical measurement, from a minimum of 8 to a maximum of about 50 periods of the 400-Hz wave were collected per diode, depending on the light intensity in the tissue. Each period of the 400-Hz wave is digitized at 16 points. All the collected periods at 400 Hz are averaged together, giving an average wave consisting of 16 points. At the end of this acquisition process, the 16-point wave is transformed using a fast Fourier transform algorithm to give the values of dc, ac, and phase of the fundamental harmonic frequency of 400 Hz. This process is repeated for each one of the light sources, yielding the values of dc, ac, and phase for all the eight LEDs. The multiplexer clock is driven by the same ISS card that performs the sampling of the photomultiplier signal, in such a way that the sampling and multiplexer clocks are synchronous. At this point, the slopes S_{dc}, S_{ac}, and S_{Φ} associated with dc, ac, and phase are computed as described elsewhere[15] (see also the appendix). Once the slopes are known, the absolute values of the scattering and absorption coefficients at the two source wavelengths are obtained using either the (Φ,dc) or the (Φ,ac) pairs (see the appendix for details). The entire process is then repeated to provide continuous monitoring of the scattering and absorption coefficients values. From the absorption coefficients, one can calculate the absolute concentrations of the oxy- and deoxyhemoglobin using the relationships (2) and (3). From the concentration of the oxy and deoxy species, the hemoglobin saturation Y and the total hemoglobin content (THC) can be obtained from the following relationships:

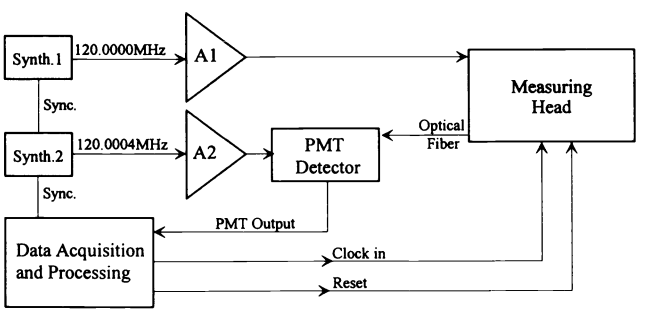

Fig. 4 Block diagram of the frequency-domain tissue spectrometer.

$$Y=\frac{[HbO_2]}{[Hb]+[HbO_2]}\times 100\%$$

$$=\frac{\varepsilon_{Hb}^{\lambda_2}-\varepsilon_{Hb}^{\lambda_1}\mu_a^{\lambda_2}/\mu_a^{\lambda_1}}{\varepsilon_{Hb}^{\lambda_2}-\varepsilon_{HbO_2}^{\lambda_2}+\left(\varepsilon_{HbO_2}^{\lambda_1}-\varepsilon_{Hb}^{\lambda_1}\right)\mu_a^{\lambda_2}/\mu_a^{\lambda_1}}\times 100\% \ , \qquad (4)$$

$$THC=[Hb]+[HbO_2] \ . \qquad (5)$$

The above discussion requires that the four LEDs at the same wavelength be identical: same dc_0, ac_0, Φ_0 (dc, ac, Φ measured at $r=0$). This is not the case, because the LEDs can differ one from another and, as already discussed, we

Downloaded From: http://proceedings.spiedigitallibrary.org/ on 08/29/2016 Terms of Use: http://spiedigitallibrary.org/ss/termsofuse.aspx

accomplished light-source equilibration by driving each LED with different currents. Therefore, we must calibrate the light intensity and the phase of the eight light sources. The calibration is performed by placing the measurement head on a solid block of a substance of known absorption and scattering coefficients. The values of the optical properties of the calibration block (made of a polymerizable glue) are measured by using a single intensity-modulated light source. This light source is placed on the surface of the block and is moved to different positions with respect to the detector (which is also placed on the surface of the block) to provide data relative to several source-detector separations. The diffusion model for the semi-infinite geometry (see the appendix and Ref. 15) is then applied to obtain μ_a and μ_s' at the wavelength of the light source. In this fashion, we obtained the following values for the optical parameters of the calibration block at the two wavelengths of interest: $\mu_a(715\ \text{nm}) = 0.021\ \text{cm}^{-1}$, $\mu_a(850\ \text{nm}) = 0.024\ \text{cm}^{-1}$, $\mu_s'(715\ \text{nm}) = 1.94\ \text{cm}^{-1}$, $\mu_s'(850\ \text{nm}) = 1.63\ \text{cm}^{-1}$. It is desirable that the optical properties of the calibration block be similar to those of the investigated sample. In this way, the light intensity detected on the sample is similar to that collected on the calibration block.

When the measuring head of the tissue oximeter is placed on the calibration block, multiplicative factors for the dc and ac intensities and additive factors for the phases of the light sources are introduced in the computer in order to reproduce the known values of μ_a and μ_s'. Note that this calibration is performed with the purpose of determining the intensity and the phase of each light source. This calibration procedure should not be confused with the calibration of most commercial oximeters, which need to be calibrated according to 0-to-100% baselines and statistical tables based on the spectroscopic characteristics of the particular tissue to be measured. We also periodically checked the light-source calibration for drifts in the light-source characteristics.

A photograph of a prototype of the instrument measurement head is shown in Fig. 5.

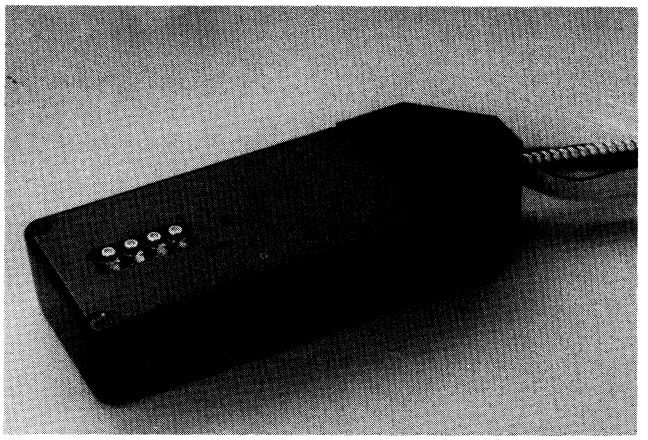

Fig. 5 Photograph of a prototype of the measuring head of the frequency-domain tissue spectrometer built by ISS, Inc. (Champaign, Illinois).

3 Instrument Performance

3.1 *Precision*

The precision of the μ_a and μ_s' determination depends on the level of the detected signal and on the acquisition time. We pointed out that we are injecting more current in the more distant LEDs so as to have comparable signals from all of the light sources. We define the acquisition time t_a to be the time required to obtain μ_a and μ_s' at both λ_1 and λ_2. We have verified that the instrument is shot-noise limited, so that the precision varies as the square root of the product of detected signal and acquisition time. To quantify the precision of the instrument, we have measured μ_a and μ_s' at a signal level of about 10% of the full-scale signal (i.e., the signal that saturates the analog-to-digital converter) and for different acquisition times. The experiment was performed on the same solid block used to perform the light calibration procedure. The estimated relative standard deviation uncertainties σ in μ_a and μ_s' are plotted in Fig. 6 as a function of acquisition time.

The standard-deviation uncertainties in μ_a and μ_s' can be propagated through Eqs. (2), (3) to yield the uncertainties in $[HbO_2]$ and [Hb]. The uncertainties in Y and THC can then be obtained from Eqs. (4) and (5). The results are the following:

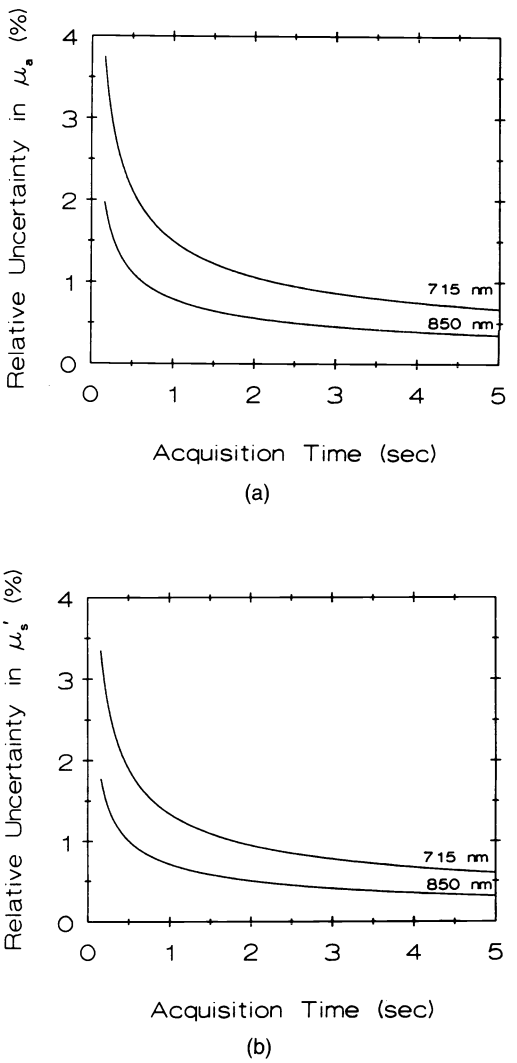

Fig. 6 Relative standard deviation uncertainties for (a) μ_a and (b) μ_s' as a function of acquisition time at a signal level of about 10% of the full-scale signal.

Downloaded From: http://proceedings.spiedigitallibrary.org/ on 08/29/2016 Terms of Use: http://spiedigitallibrary.org/ss/termsofuse.aspx

$$\sigma([HbO_2]) = \left[\left(\frac{\varepsilon_{Hb}^{\lambda_2}}{\Delta} \right)^2 \sigma^2\left(\mu_a^{\lambda_1} \right) + \left(\frac{\varepsilon_{Hb}^{\lambda_1}}{\Delta} \right)^2 \sigma^2\left(\mu_a^{\lambda_2} \right) \right]^{1/2} , \quad (6)$$

$$\sigma([Hb]) = \left[\left(\frac{\varepsilon_{HbO_2}^{\lambda_2}}{\Delta} \right)^2 \sigma^2\left(\mu_a^{\lambda_1} \right) + \left(\frac{\varepsilon_{HbO_2}^{\lambda_1}}{\Delta} \right)^2 \sigma^2\left(\mu_a^{\lambda_2} \right) \right]^{1/2} , \quad (7)$$

$$\sigma(Y) = Y \frac{[Hb]}{[Hb] + [HbO_2]} \left[\left(\frac{\sigma([HbO_2])}{[HbO_2]} \right)^2 + \left(\frac{\sigma([Hb])}{[Hb]} \right)^2 \right]^{1/2} , \quad (8)$$

$$\sigma(THC) = \{ \sigma^2([HbO_2]) + \sigma^2([Hb]) \}^{1/2} , \quad (9)$$

where $\Delta = (\varepsilon_{HbO_2}^{\lambda_1} \varepsilon_{Hb}^{\lambda_2} - \varepsilon_{HbO_2}^{\lambda_2} \varepsilon_{Hb}^{\lambda_1})$.

3.2 *Accuracy*

The accuracy of the instrument is the capability of measuring values of μ_a and μ_s' that reproduce the actual values of μ_a and μ_s' of the medium. Several factors influence the accuracy:

1. validity of the physical model
2. cross talk between channels
3. optical coupling between the light sources and the medium
4. wide spectral emission of the LEDs.

1: The accuracy of the employed relationships between the frequency-domain parameters (dc, ac, and phase) and the optical properties of the medium (μ_a, μ_s', and the index of refraction) relies on the validity of the assumptions made in deriving them. These assumptions are the macroscopic homogeneity of the medium and the semi-infinite geometry.[15] Neither condition is rigorously satisfied in the case of *in vivo* measurements. Nevertheless, it has been proposed that some tissues can be treated as homogeneous media.[5,20] That is not true in the presence of macroscopic inhomogeneties whose optical properties are strongly different from those of the surrounding tissue, as is the case of tumors, large blood vessels, or the vicinity of bones. Moreover, the tissue must be at least several centimeters thick to permit one to apply the equations for the semi-infinite geometry. The actual air-tissue interface is not a geometrical plane, and source and detector are not located exactly on the boundary plane. However, we have demonstrated that the measured phase and dc and ac photon fluxes are largely insensitive to the precise geometrical configuration at the boundary.[15] The overall accuracy of the measurement in the macroscopically homogeneous, semi-infinite medium in the diffusion model has been shown to be better than 4% for μ_a (in the range 0.02 to 0.40 cm^{-1}) and better than 15% for μ_s' (in the range 4 to 16 cm^{-1}).[15]

2: We have minimized the cross talk between consecutive channels (corresponding to the eight light sources) by disregarding each first period of the 400-Hz cross-correlation wave after switching between LEDs. This procedure has the effect of ignoring data collected during the first 2.5 ms following the switch between two LEDs. In this way, we have achieved a measured cross talk of less than 0.5%.

3: The optical coupling between the light sources and the medium strongly affects the amount of detected light. Nonetheless, when the LEDs are all evenly coupled to the medium, the effect on the measured values of μ_a and μ_s' is on the order of a few percent. The reason this effect is so small is the insensitivity of the straight lines associated with dc, ac, and phase (which are employed for determining μ_a and μ_s') to the light-source intensity. In regard to *in vivo* applications, we have determined that the physical contact of the LEDs with the skin is not critical. This insensitivity, which is very important for quantitative measurements, is shown in Fig. 7, where we report the results obtained for the dc intensity, $\mu_a(\lambda_1)$, $\mu_a(\lambda_2)$, $\mu_s'(\lambda_1)$, and $\mu_s'(\lambda_2)$ in four different conditions of optical coupling between LEDs and tissue. By contrast, when the optical coupling is not equal for the eight LEDs, the measured values of μ_a and μ_s' can be affected by systematic error. This error, estimated to be less than about 20%, must be considered when the LED-skin contact is varied unevenly over the eight LEDs.

4: Rigorously, the equations utilized to calulate μ_a and μ_s' are valid only if monochromatic light is employed. The wide spectral emission of the LEDs (about 40 nm FWHM) introduces contributions to the measured frequency-domain parameters that are not taken into account by our theoretical model. However, the single-wavelength equations are still exact if the absorption and reduced scattering coefficients of the medium are wavelength independent. In tissues, μ_s' is actually[11] a weak function of λ, but μ_a is wavelength dependent (even though the opposite spectral dependencies of HbO_2 and Hb in the region from 700 to 900 nm partially compensate). We have simulated a realistic condition for biological tissues in conjunction with a light-source spectral distribution typical of an LED and with the spectral response of our detector. We have found that by using the single-wavelength equations in these experimental conditions, μ_a

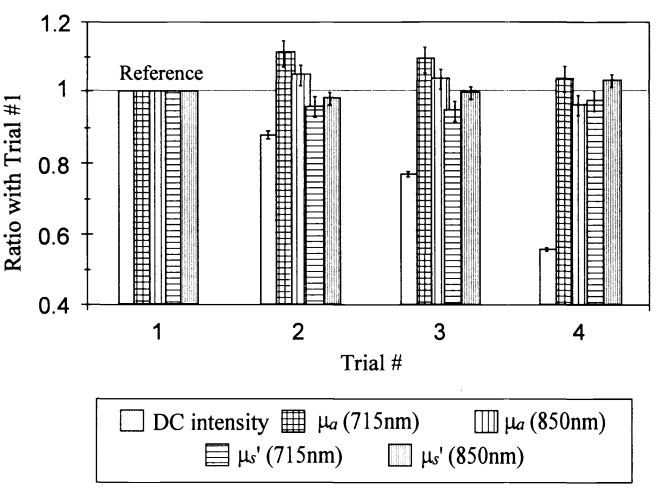

Fig. 7 Evaluation of the sensitivity of the measured optical coefficients to the optical coupling between LEDs and tissue. The instrument was located on the thigh of a human subject. In trial 1 a firm pressure was applied, and this pressure was progressively decreased between successive trials. In trial 4 the LEDs were barely touching the skin. Considering trial 1 as a reference, one can observe that though the pressure strongly affects the detected intensity, it has little effect on the measured values of absorption and scattering coefficients.

Downloaded From: http://proceedings.spiedigitallibrary.org/ on 08/29/2016 Terms of Use: http://spiedigitallibrary.org/ss/termsofuse.aspx

at 715 nm is overestimated by about 5%, but at 850 nm is underestimated by about 3%. The effect on μ_s' is less than 1%. We note that the systematic error due to the wide spectral emission of the source depends only on spectral shapes of $\mu_a(\lambda)$, $\mu_s'(\lambda)$, $S(\lambda)$, and $F(\lambda)$ (where S is the source intensity and F is the spectral response of the detector). Any scale factors in S and F, which may depend for instance on the LED-tissue optical coupling or on the voltage supplied to the PMT, have no effect on the calculated values of μ_a and μ_s'. Such scale factors cancel out in the deviation of μ_a and μ_s'. The use of laser diodes as the light sources would eliminate this bandwidth-dependent contribution to the instrumental accuracy.

4 Test *in Vitro*

We have tested our instrument by measuring the optical coefficients of a tissuelike phantom consisting of an aqueous solution of Liposyn 20% (from Abbott Laboratories) and black India ink. The medium was held in a 3.8-l cylindrical container 20 cm in diameter. We employed several concentrations of Liposyn (13 to 50 ml/l) to vary μ_s', and different concentrations of a prediluted black India ink solution (0.26 to 1.06 ml/l) to vary μ_a. In this way we tested the instrument over a range of values of μ_a and μ_s'. Specifically, we conducted eight measurements: the first four relative to four different Liposyn concentrations in the absence of black India ink, and the last four relative to four different ink concentrations and the same Liposyn concentration of 50 ml/l. The conditions for each of the eight measurements are listed in Table 1. The measuring head was placed on the surface of the turbid medium, and we verified that its positioning with respect to the surface is not critical. The measured values of μ_a and μ_s' are essentially unaffected by slightly tilting, raising, or lowering the head relative to the surface. To evaluate the accuracy of the measurements, we have also measured μ_a and μ_s' in a quasi-infinite geometry by deeply immersing a single LED and the detector optical fiber inside the medium. In this case, multiple source-detector separations were accomplished by physically moving the LED to different positions relative to the detector fiber. This technique has already been described, and it provides accurate values for μ_a and μ_s'. We have estimated that in these specific experimental conditions (Liposyn as the scattering substance, water and black India ink as the absorbers, known LED emission and PMT gain-function spectral shapes) the systematic error introduced by using the single-wavelength equations is within the measurement noise. The experimental results for μ_a and μ_s' are shown in Figs. 8 and 9 respectively. Since the results in the infinite geometry are known to be accurate,[12,14] Figs. 8 and 9 provide information on the accuracy of the instrument, on its ability to separate the absorption from the scattering properties of the medium, and on the lack of correlation when one of the two parameters is changed while the other is kept constant.

5 Test *in Vivo*

Some of the results already presented were obtained from *in vivo* measurements. Specifically, the study of the effect of the optical coupling between LEDs and tissues (see Fig. 7) was conducted by applying the instrument on the thigh of a human subject.

Table 1 Liposyn and black India ink concentrations in the eight *in vitro* measurements.

Meas. #	Liposyn conc. (ml/l)	Black India ink conc.(*) (ml/l)
1	13 ± 1	0
2	26 ± 1	0
3	38 ± 2	0
4	50 ± 2	0
5	50 ± 2	0.26 ± 0.01
6	50 ± 2	0.53 ± 0.02
7	50 ± 2	0.79 ± 0.03
8	50 ± 2	1.06 ± 0.04

(*) The absorber concentrations in the Table refer to a prediluted black India ink solution and not to pure black India ink.

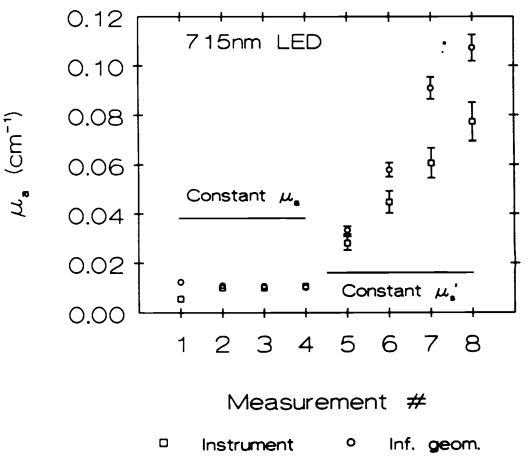

(a)

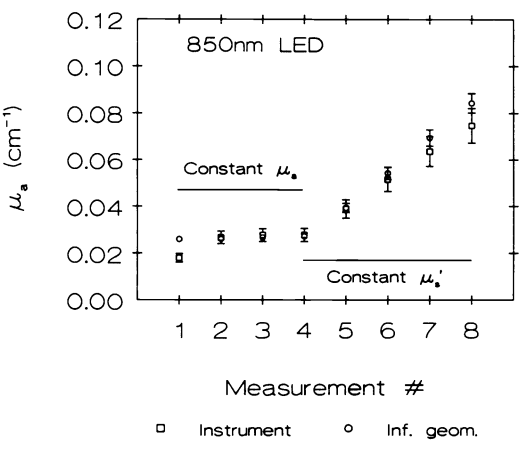

(b)

Fig. 8 Measurement of μ_a of a model scattering and absorbing medium (aqueous solution of Liposyn 20% and black India ink) using (a) the 715 nm LEDs and (b) the 850 nm LEDs. In measurements 1–4 the solution contains no ink; in measurements 4–8 the scatterer content is kept constant (refer to Table 1 for the specific experimental conditions in each measurement). The values measured with our instrument (□) are compared with the values obtained deep in the medium (○).

Downloaded From: http://proceedings.spiedigitallibrary.org/ on 08/29/2016 Terms of Use: http://spiedigitallibrary.org/ss/termsofuse.aspx

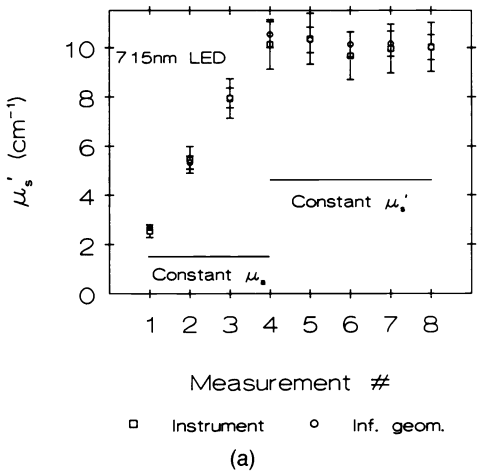

Fig. 9 Measurement of μ_s' of a model scattering and absorbing medium (aqueous solution of Liposyn 20% and black india ink) using (a) the 715-nm LEDs and (b) the 850-nm LEDs. Refer to the caption of Fig. 8 and to Table 1 for details on the experimental conditions in each measurement. The values measured with our instrument (□) are compared with the values obtained deep in the medium using an established technique (○).

We have also used our instrument to measure the temporal behavior of the oxygenation of the forearm skeletal muscle during ischemia. For this purpose the instrument was placed on the forearm of a volunteer and a pneumatic cuff was used to induce a vascular occlusion causing ischemia. In the measurement protocol, after one minute of baseline acquisition, the cuff was inflated to a pressure of 240 to 260 mm Hg and kept inflated for eight minutes. Then, the cuff was released and data acquired for three more minutes. The acquisition time was set to 1 s. The result for the temporal evolution of hemoglobin saturation during this experimental protocol *in vivo* is shown in Fig. 10.

6 Discussion

First we examine the *in vitro* results reported in Figs. 8 and 9.

For *measurements 1–4*, in the absence of black India ink (i.e., at low values of μ_a), the agreement between the infinite-geometry results and the instrument readings is very good. The value of μ_a is essentially due to the absorbance of water

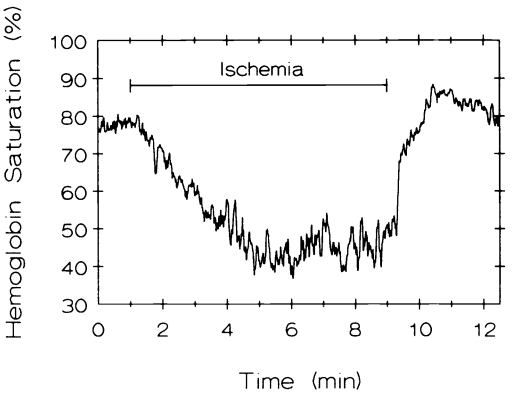

Fig. 10 Temporal evolution of hemoglobin saturation of the forearm skeletal muscle during ischemia.

at the measured wavelength. We point out that the spectral response of the PMT we employed (Hamamatsu R928) plays a role here. While that response is relatively constant in the region from 660 to 760 nm, it drops by more than one order of magnitude from 800 to 900 nm. Taking into account the photomultiplier response, the measured peak wavelengths of the LEDs we utilized are 715 and 825 nm. The values of the absorption coefficients of water at 715 and 825 nm (0.0088 and 0.028 cm^{-1}, respectively[21]) are close to the values we measured in the absence of ink. Note that the measured values of μ_a are not affected by Liposyn content, which increases linearly from measurement 1 to measurement 4. By contrast, μ_s' linearly increases as a function of scatterer concentration, as expected.

In *measurements 5–8,* the second series, in which black India ink was added to increase μ_a, the instrument readings for μ_a start to deviate from the infinite-geometry results. These deviations systematically increase with increasing μ_a and are larger for the 715-nm LEDs than for the 850-nm LEDs. The maximum deviation (measurement 8) is about 25% for the 715-nm LED, and about 12% for the 850-nm LED. On the other hand, the instrument readings for μ_s' essentially reproduce the infinite-geometry results. The expected qualitative results (linear dependence of μ_a and non-dependence of μ_s' on ink concentration) are reproduced. The deviation between the values of μ_a measured with our tissue spectrometer and the results obtained in the infinite geometry (see Fig. 8) are larger than expected. These deviations should have been less[15] than 4%. We ascribe this effect to the fact that we covered the surface of the measuring head with a thin layer of transparent flexible plastic to protect the device from contamination by the liquid phantom. This layer could wrinkle, causing unpredictable (even if small) effects on its transmission properties. We performed a few measurements without the protective coating. In this case, the deviations between the instrument readings and the infinite geometry results were within the expected range. Since the prototype measurement head is not waterproof, an extended series of measurements on a liquid phantom is not possible with it. Measurements on human tissues, however, do not pose this problem.

On the basis of these experimental results and of the discussion in Sec. 3, we have estimated the uncertainties in the measured quantities μ_a, μ_s', Y, [HbO_2], [Hb], and THC. We

Downloaded From: http://proceedings.spiedigitallibrary.org/ on 08/29/2016 Terms of Use: http://spiedigitallibrary.org/ss/termsofuse.aspx

distinguish the case of an absolute measurement, in which a direct reading is considered, from the case of a differential measurement, in which the difference between two readings is considered. In the latter case there is no contribution from systematic errors, and the uncertainties are due to instrument noise. Our estimates for the uncertainties relative to 1-s acquisition time and 10% of the full-scale signal are reported in Table 2. The differential measurement statistical errors in μ_a and μ_s' are propagated quadratically through Eqs. (2), (3), (4), (5) to obtain the errors in [HbO_2], [Hb], Y, and THC [see Eqs. (6) through (9)]. The absolute measurement systematic errors in μ_a and μ_s' are propagated linearly through Eqs. (2), (3), and (5) to obtain the errors in [HbO_2], [Hb], and THC. The absolute measurement error in Y is obtained from Eq. (4) by considering the errors in $\mu_a^{\lambda 1}$ and $\mu_a^{\lambda 2}$ to be dependent. We observe that the error in the absolute determination of the hemoglobin saturation Y is not much larger than the uncertainty due to the instrument noise. This fact is due to the particular dependence of Y on $\mu_a^{\lambda 1}$ and $\mu_a^{\lambda 2}$. As shown by Eq. (4), Y depends only on the ratio $\mu_a^{\lambda 2}/\mu_a^{\lambda 1}$, and a systematic error in both $\mu_a^{\lambda 1}$ and $\mu_a^{\lambda 2}$ has little effect on their ratio. This is particularly true in our case, since the ratio $\mu_a^{\lambda 2}/\mu_a^{\lambda 1}$ is on the order of unity. The instrumental limit is given by the statistical errors in the third column of Table 2. If one considers that typical values of the measured quantities in tissue are $\mu_a \sim 0.1\ cm^{-1}$, $\mu_s' \sim 10\ cm^{-1}$, $Y \approx 70\%$, [HbO_2] ~ [Hb] ~ 10 to 100 μM, the errors given by instrumental noise are of the order of a few percent. This is certainly a clinically acceptable uncertainty. On the other hand, the systematic errors (whose maximum estimate is reported in column 2 of Table 2), which are due to the validity of the physical model and to uneven optical coupling between LEDs and tissue, can be quite large. However, being systematic, they can be minimized by applying appropriate corrections.

The *in vivo* results shown in Fig. 10 are reported here to support the feasibility of *in vivo* applications of our spectrometer. We limit the discussion of these results to two considerations. First, similar variations of hemoglobin saturation have been reported in the literature.[22] Second, the absolute value of Y is an average over the tissue and is not the value relative to blood. A more complete and systematic *in vivo* study conducted with our tissue spectrometer is reported in a separate paper.[23]

7 Conclusion

Since the early decades of this century, it has been proposed that the near-infrared absorption band of hemoglobin could be used to measure hemoglobin saturation directly and non-invasively.[24,25] The basic idea is to exploit the differential absorption of the oxygenated and deoxygenated forms of hemoglobin in the 700- to 900-nm spectral region. Several instruments based on steady-state differential absorption have been proposed.[24–26] Although some of those instruments have been fairly successful and have found regular use in clinical practice, all of them suffer from a major problem, namely, that simple differential absorption cannot compensate for the different scattering properties of the different tissues and the variability of the scattering coefficient for the same tissue among individuals. To partially overcome this intrinsic limitation of the differential absorption method, it was proposed to use more than two absorption wavelengths or the entire absorption spectrum in the 700- to 900-nm region.[27] Even with this improvement, the determination of tissue oxygenation and total hemoglobin content needed some sort of *a priori* calibration based on empirical tables that statistically account for individual and time variability.

During the 1980s a new possibility arose, due to the development of picosecond lasers with emission in the spectral region of the near-infrared hemoglobin absorption. It was shown that, by a measurement of the time of flight of a light pulse between the source fiber and the detector fiber, it was possible to determine separately the scattering and absorption coefficients of the medium.[5] A new series of instruments was proposed depending on the method used to measure the time of flight. Notable are the instruments proposed by Chance et al. using the frequency domain method at a single modulation frequency.[28,29] However, this method does not entirely solve the problem mentioned, since it is based on a differential phase measurement. The quantity measured by all the above instruments is always the relative oxygenation of tissues. They cannot determine the absolute values of μ_a and μ_s'.

On the other hand, the instrument we have designed provides quantitative absolute measurements of the absorption and scattering coefficients with relatively high accuracy. It then permits one to determine the absolute values of the concentrations of oxy- and deoxyhemoglobin, and of the oxygenation in tissues. The measured quantities (μ_a, μ_s', [HbO_2], [Hb], Y, THC) are displayed directly on a screen, providing a simultaneous real-time monitoring of these tissue parameters. Time derivatives and time integrals of the measured quantities can be monitored in real time as well. Hemoglobin saturation results obtained *in vivo* in a systematic study are presented in a separate paper.[23] Our instrument can also be compact. All the required instrumentation shown in Fig. 4 can fit in a light and portable unit.

There are several characteristics of our instrument that can be changed without affecting the underlying principle ideas:

- The number of light sources can be augmented or decreased according to the application. For hemoglobin saturation measurement, eight sources are adequate. However, the same multiplexing principle can be applied to a much larger number of sources for the simultaneous determination of the concentration of more chromophores, for adding another wavelength, or for imaging applications.

- We have used light-emitting diodes as the light sources. It is possible to replace them with laser diodes, with minor modifications of the driving electronics. The ad-

Table 2 Estimated uncertainties in the measured quantities for 1-s acquisition time and 10% of the full-scale signal.

Quantity	Absolute Measurement Uncertainty(*) (Systematic) (due to absolute accuracy)	Differential Measurement Uncertainty (Statistical) (due to instrument noise)
μ_a (cm^{-1})	0.012 cm^{-1}	0.001 cm^{-1}
μ_s' (cm^{-1})	1.5 cm^{-1}	0.1 cm^{-1}
Y (%)	8%(**)	3%(**)
[HbO_2] (μM)	35 μM	3 μM
[Hb] (μM)	20 μM	2 μM
THC (μM)	55 μM	4 μM

(*) Calculated for μ_a=0.08 cm^{-1}, μ_s'=8 cm^{-1}.
(**) Maximum value calculated for *THC*=100 μM and Y ranging from 10% to 90%.

Downloaded From: http://proceedings.spiedigitallibrary.org/ on 08/29/2016 Terms of Use: http://spiedigitallibrary.org/ss/termsofuse.aspx

vantage of laser diodes over LEDs is that laser diodes emit monochromatic light, provide higher intensity, and can be modulated at higher frequencies. However, for the purpose of the proof of concept of a multiplexed tissue oximeter, LEDs are adequate both in light intensity and in modulation frequency.

- The value of 400 Hz for the cross-correlation frequency was selected for convenience. We have experimentally tested cross-correlation frequencies from 40 to 1500 Hz, with comparable results. The use of higher values of the cross-correlation frequency allows for a better detection of faster processes.
- The light-source multiplexer was constructed using mechanical relays (see Fig. 3). However, solid-state switches can be used if multiplexing speeds faster than 2.5 ms are required.

8 Appendix: Measurement Protocol Based on Multiple Source-Detector Separations

In the infinite geometry, the measurable quantities $\ln(rU_{dc})$, $\ln(rU_{ac})$, and Φ are linear functions of the source-detector distance r (U_{dc} is the average photon density, U_{ac} is the amplitude of the photon density oscillations, and Φ is the phase lag between source and detector). One can write the following equations[12]:

$$\ln(rU_{dc}) = rS_{dc}(\mu_a,\mu_s') + K_{dc} \ , \tag{10}$$

$$\ln(rU_{ac}) = rS_{ac}(\mu_a,\mu_s') + K_{ac} \ , \tag{11}$$

$$\Phi = rS_{\Phi}(\mu_a,\mu_s') + K_{\Phi} \ , \tag{12}$$

where the slopes S_{dc}, S_{ac}, S_{Φ} are functions of the optical coefficients μ_a, μ_s', while K_{dc}, K_{ac}, K_{Φ} are independent of r. Once the slopes are mesured, μ_a and μ_s' can be obtained either from the (S_{dc}, S_{Φ}) or from the (S_{ac}, S_{Φ}) pair by employing analytical expressions.[14] For instance, if the dc intensity and phase are the measured quantities, the following equations yield μ_a and μ_s':

$$\mu_a = -\frac{\omega}{2\nu}\frac{S_{dc}}{S_{\Phi}}\left(\frac{S_{\Phi}^2}{S_{dc}^2}+1\right)^{-1/2} \ , \tag{13}$$

$$\mu_s' = \frac{S_{dc}^2}{3\mu_a} - \mu_a \ , \tag{14}$$

where $\omega/2\pi$ is the modulation frequency and ν is the velocity of light in the medium.

The problem in the semi-infinite geometry, where source and detector are placed on the surface of the medium, is more complicated but formally identical. Eqs. (10), (11), (12) are replaced by the following equations[15]:

$$f(r,U_{dc},\mu_a,\mu_s') = rS_{dc}(\mu_a,\mu_s') + K_{dc}' \ , \tag{15}$$

$$g(r,U_{ac},\mu_a,\mu_s') = rS_{ac}(\mu_a,\mu_s') + K_{ac}' \ , \tag{16}$$

$$h(r,\Phi,\mu_a,\mu_s') = rS_{\Phi}(\mu_a,\mu_s') + K_{\Phi}' \ , \tag{17}$$

where f, g, h are known functions of their arguments and K_{dc}', K_{ac}', K_{Φ}' are independent of r. Note that the slopes S_{dc}, S_{ac}, S_{Φ} in Eqs. (15)–(17) are the same as in Eqs. (10)–(12). Consequently, one can determine μ_a and μ_s' from Eqs. (13), (14) also in the semi-infinite geometry. The problem of the presence of μ_a and μ_s' in the left-hand sides of Eqs. (15)–(17) is circumvented by employing an iterative procedure. First, the terms containing μ_a and μ_s' in the functions f, g, h are neglected and the zeroth-order slopes $S_{dc}^{(0)}$, $S_{ac}^{(0)}$, $S_{\Phi}^{(0)}$ are obtained. Equation (13), (14) provide the zeroth-order $\mu_a^{(0)}$ and $\mu_s'^{(0)}$, which are used in the left-hand sides of Eqs. (15), (16), (17) to obtain $S_{dc}^{(1)}$, $S_{ac}^{(1)}$, $S_{\Phi}^{(1)}$ and hence $\mu_a^{(1)}$, $\mu_s'^{(1)}$. This procedure can be applied recursively until $\mu_a^{(i)}$ and $\mu_s'^{(i)}$ reproduce themselves within a given uncertainty. Convergence is typically reached after three to five iterations. The same values of μ_a and μ_s' are reached as a result of the iterative procedure, independently of the choice for the starting values of μ_a and μ_s'.

Acknowledgments

The authors thank Roberto de Blasi and Marco Ferrari for their collaboration in the *in vivo* measurements reported in Fig. 10. They are also grateful to William Mantulin for his valuable suggestions. The experimental work, as well as the analysis of the data, was performed at the Laboratory for Fluorescence Dynamics (LFD) in the Department of Physics at the University of Illinois at Urbana-Champaign (UIUC). The LFD is supported jointly by the Division of Research Resource of the National Institutes of Health (RR03155) and UIUC, and this research was supported by grant CA 57032 (EG).

References

1. Special issues on "Biomedical Optics," *Appl. Opt.* **28** (June 1989); *Appl. Opt.* **32**(Feb. 1993); *Opt. Eng.* **32** (Feb. 1993).
2. M. Cope, P. van der Zee, M. Essenpreis, S. R. Arridge, and D. T. Delpy, "Data analysis methods for near infrared spectroscopy of tissues: problems in determining the relative cytochrome aa_3 concentration," *Proc. SPIE* **1431,** 251–263 (1991).
3. F. F. Jöbsis, J. H. Keizer, J. C. LaManna, and M. Rosenthal, "Reflectance spectrophotometry of cytochrome aa_3 *in vivo*," *J. Appl. Physiol.* **43,** 858–872 (1977).
4. T. J. Farrel, M. S. Patterson, and B. Wilson, "A diffusion theory model of spatially resolved, steady-state diffuse reflectance for the noninvasive determination of tissue optical properties *in vivo*," *Med. Phys.* **19,** 879–888 (1992).
5. M. S. Patterson, B. Chance, and B. C. Wilson, "Time resolved reflectance and transmittance for the non-invasive measurement of optical properties," *Appl. Opt.* **28,** 2331–2336 (1989).
6. S. R. Andersson-Engels, R. Berg, S. Svanberg, and O. Jarlman, "Time-resolved transillumination for medical diagnostic," *Opt. Lett.* **15,** 1179–1181 (1990).
7. D. Benaron and D. K. Stevenson, "Optical time-of-flight and absorbance imaging of biological media," *Science* **259,** 1463–1466 (1993).
8. E. Gratton, W. W. Mantulin, M. J. van de Ven, and J. B. Fishkin, "A novel approach to laser tomography," *Bioimaging* **1,** 40–46 (1993).
9. M. S. Patterson and B. C. Wilson, "The propagation of optical radiation in tissues," *Lasers Med. Sci.* **6,** 115–168, 379–396 (1991).
10. J. B. Fishkin, E. Gratton, M. J. vandeVen, and W. W. Mantulin, "Diffusion of intensity modulated near-IR light in turbid media," *Proc. SPIE* **1431,** 122–135 (1991).
11. E. M. Sevick, B. Chance, J. Leigh, S. Nioka, and M. Maris, "Quantitation of time- and frequency resolved optical spectra for the determination of tissue oxygenation," *Anal. Biochem.* **195,** 330–351 (1991).
12. J. B. Fishkin and E. Gratton, "Propagation of photon-density waves in strongly scattering media containing an absorbing semi-infinite plane bounded by a straight edge," *J. Opt. Soc. Am. A* **10,** 127–140 (1993).
13. M. A. Franceschini, S. Fantini, and E. Gratton, "LEDs in frequency domain spectroscopy of tissues," *Proc. SPIE* **2135,** 300–306 (1994).
14. S. Fantini, M. A. Franceschini, J. B. Fishkin, B. Barbieri, and E. Gratton, "Quantitative determination of the absorption spectra of chromophores in strongly scattering media: a light-emitting-diode based technique," *Appl. Opt.* **33,** 5204–5213 (1994).

Downloaded From: http://proceedings.spiedigitallibrary.org/ on 08/29/2016 Terms of Use: http://spiedigitallibrary.org/ss/termsofuse.aspx

15. S. Fantini, M. A. Franceschini, and E. Gratton, "Semi-infinite geometry boundary problem for light migration in highly scattering media: a frequency-domain study in the diffusion approximation," *J. Opt. Soc. Am. B.* **11,** 2128–2138 (1994).
16. D. T. Delpy, M. Cope, P. van der Zee, S. Arridge, S. Wray, and J. Wyatt, "Estimation of optical pathlength through tissue from direct time of flight measurement," *Phys. Med. Biol.* **33,** 1433–1442 (1988).
17. H. Miyake, S. Nioka, A. Zaman, D. S. Smith, and B. Chance, "The detection of cytochrome oxidase heme iron and copper absorption in the blood-perfused and blood-free brain in normoxia and hypoxia," *Anal. Biochem.* **192,** 149–155 (1991).
18. B. L. Horecker, "The absorption spectra of hemoglobin and its derivatives in the visible and near infra-red regions," *J. Biol. Chem.* **148,** 173–183 (1943).
19. J. L. Boulnois, "Photophysical processes in recent medical laser developments: a review," *Lasers Med. Sci.* **1,** 47–66 (1986).
20. M. S. Patterson, J. D. Moulton, B. C. Wilson, and B. Chance, "Applications of time-resolved light scattering measurements to photodynamic therapy dosimetry," *Proc. SPIE* **1203,** 62–75 (1990).
21. G. M. Hale and M. R. Querry, "Optical constants of water in the 200 nm to 200 μm wavelength region," *Appl. Opt.* **12,** 555–563 (1973).
22. R. A. de Blasi, M. Cope, C. Elwell, F. Safoue, and M. Ferrari, "Noninvasive measurement of human forearm oxygen consumption by near infrared spectroscopy," *Eur. J. Apply Physiol.* **67,** 20–25 (1993).
23. R. A. de Blasi, S. Fantini, M. A. Franceschini, M. Ferrari, and E. Gratton, "Cerebral and muscle oxygenation saturation measurement by a novel frequency-domain near infrared spectrometer," submitted for publication.
24. G. A. Millikan, "The oximeter, an instrument for measuring continuously the oxygen saturation of arterial blood in man," *Rev. Sci. Instrum.* **13,** 434–444 (1942).
25. B. Chance, "Rapid and sensitive spectrophotometry. III. A double beam apparatus," *Rev. Sci. Instrum.* **22,** 634–638 (1951).
26. M. Cope, "Optical examination apparatus," U.S. Patent No. 5, 032, 024 (1991).
27. M. Ferrari, Q. Wei, L. Carraresi, R. de Blasi, and G. Zaccanti, "Time-resolved spectroscopy of the human forearm," *J. Photochem. Photobiol. B* **16,** 141–153 (1992).
28. B. Chance, "Phase modulated spectrophotometry," U.S. Patent No. 4,972,331 (1990).
29. B. Chance, "Phase modulated spectrophotometry," U.S. Patent No. 5,122,974 (1992).

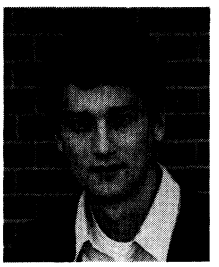

Sergio Fantini received his doctoral degree in physics at the University of Florence (Italy) in 1992. His dissertation concerned a Raman scattering study of the high-T_c superconductor YBCO. He served as an officer in the scientific laboratories of an Italian police force, conducting studies on forensic applications of optics and acoustics. Currently, he is a postdoctoral fellow at the Laboratory for Fluorescence Dynamics at the University of Illinois at Urbana-Champaign (UIUC). His work is focused on the study of light propagation in turbid media and the development of measurement techniques of medical interest.

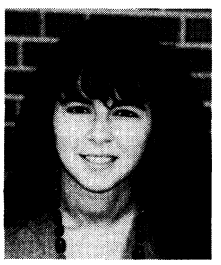

Maria Angela Franceschini-Fantini received her doctoral degree in physics at the University of Florence (Italy) in 1992. Her dissertation concerned a study of the electric discharge stability in an excimer laser. She collaborated with the Istituto di Elettronica Quantistica (CNR) in Florence to develop a long-pulse excimer laser prototype for medical applications. Currently, she is a postdoctoral fellow at the Laboratory for Fluorescence Dynamics at the University of Illinois at Urbana Champaign (UIUC). Her research is dedicated to the development of spectroscopy and imaging frequency-domain instruments for medical applications.

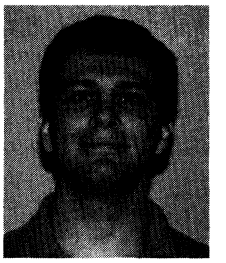

John S. Maier received his BS degree in physics in 1990 from the University of Notre Dame in South Bend, Indiana, and his MS degree in physics from the University of Illinois at Urbana-Champaign in 1991. He is enrolled in the Medical Scholars Program at the University of Illinois at Urbana-Champaign, pursuing a PhD in physics and an MD degree. Currently he is studying photon migration and its application to medical imaging and spectroscopy at the Laboratory for Fluorescence Dynamics, in the University of Illinois at Urbana-Champaign Department of Physics.

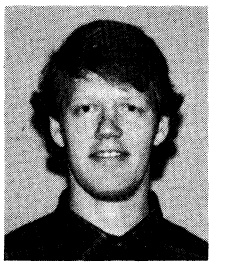

Scott A. Walker received his BA degree in physics in 1989 from Whitman College in Walla Walla, Washington, and his MS degree in physics from the University of Illinois at Urbana-Champaign in 1992. From 1989 to 1990 he worked at Los Alamos National Laboratory in the Space Science and Technology division. Currently he is working toward a PhD in physics, studying photon migration and its application to medical imaging and spectroscopy, at the Laboratory for Fluorescence Dynamics in the Department of Physics at the University of Illinois at Urbana-Champaign.

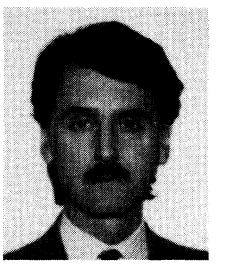

Beniamino Barbieri has been president of ISS, Inc., since 1989. He graduated with a degree in physics from the University of Pisa, Italy, in 1983, where he worked as a researcher in the Chemical Engineering Department until 1985. He joined ISS in 1985 and was involved in the development of the first fully automated multifrequency cross-correlation phase and modulation fluorometer. His present interests include the development and the application of phase fluorometry for medical diagnostics and the automation of data analysis.

Enrico Gratton received his doctorate in physics from the University of Rome in 1969. From 1969 to 1971 he was a postdoctoral fellow at the Istituto Superiore di Sanità in Italy. He came to the University of Illinois at Urbana-Champaign (UIUC) in 1976 and began his work as a research associate in the Department of Biochemistry. In 1978, he was appointed assistant professor in the Department of Physics of UIUC. In 1989, he was promoted to professor. Dr. Gratton's laboratory has reached international recognition for the development of instrumentation for time-resolved fluorescence spectroscopy using frequency-domain methods. His research interests include the design of new fluorescence instruments, protein dynamics, hydration of proteins, and IR spectroscopy of biological substances. Dr. Gratton has authored or coauthored over 130 publications in refereed scientific journals.

Downloaded From: http://proceedings.spiedigitallibrary.org/ on 08/29/2016 Terms of Use: http://spiedigitallibrary.org/ss/termsofuse.aspx